ELSEVIER

# Deconvolution of ultrafast kinetic data with inverse filtering

Ákos Bányász[a,b], Edit Mátyus[a], Ernő Keszei[a,*]

[a]*Department of Physical Chemistry, Eötvös University, P.O. Box 32, H-1518 Budapest 112, Hungary*
[b]*Research Institute for Solid State Physics and Optics, Hungarian Academy of Sciences, P.O. Box 49, H-1525 Budapest, Hungary*

## Abstract

Due to limitations of pulse widths in ultrafast laser or electron pulse kinetic measurements, in the case of subpicosecond characteristic times of the studied reactions, deconvolution with the pulses always distorts the kinetic signal. Here, we describe inverse filtering based on Fourier transformations to deconvolve measured ultrafast kinetic data without evoking a particular kinetic mechanism. Deconvolution methods using additional Wiener filtering or two-parameter regularization are found to give reliable results for simulated as well as experimental data.
© 2004 Published by Elsevier Ltd.

## 1. Introduction

Since the invention of pulse radiolysis and flash photolysis methods, a commonly encountered problem has been the finite width of the pulses used to initiate reactions, and later also the width of the light pulse used for the spectral detection of the temporal evolution of the reactions. If the relevant timescale of the studied reactions is in the same range as the widths of these pulses, the measured kinetic curves are distorted by the convolution with the pulse or lamp profile (Chase and Hunt, 1975; McKinnon et al., 1977; O'Connor et al., 1979). With the advent of subpicosecond laser and electron pulses, time resolution increased substantially. However, as a reasonably narrow spectral energy range is required both for excitation and detection of the reacting system, the temporal width of the pulses cannot be much smaller than about 100 fs, due to limitations imposed by the uncertainty relation between spectral

and temporal widths of the pulses (for example, see Donoho and Stark, 1989). As many elementary reactions occur at hundreds of femtoseconds timescale, the problem of convolution cannot be neglected in these experiments. As a result, detected absorbances can be expressed by a double integral

$$A^\lambda(\tau) = \int_{-\infty}^{\infty} I_m(\tau - t') \int_{-\infty}^{\infty} I_e^n(t) f^\lambda(t' - t) \, dt \, dt' \qquad (1)$$

that can be rewritten as

$$A^\lambda(\tau) = \mathrm{corr}(I_m, I_e^n) \otimes f^\lambda. \qquad (2)$$

The correlation of the exciting pump pulse $I_e$ (raised to the power $n$ describing $n$-photon excitation) with the measuring probe pulse $I_m$ can be considered as an effective pulse (in reality, it is somewhat broadened due to the dispersion of the refractive index between the pump and the probe wavelengths). The detected signal $A^\lambda(\tau)$ is the convolution of this effective pulse with the instantaneous kinetic response function $f^\lambda$, where $\lambda$ refers to the detection wavelength. In case of absorbance

*Corresponding author. Tel.: +36 1 209 0591; fax: +36 1 209 0602.

*E-mail address:* keszei@chem.elte.hu (E. Keszei).

detection, the kinetic response function is the sum

$$f^{\lambda}(t) = l \sum_{i=1}^{r} \varepsilon_i^{\lambda} c_i(t), \tag{3}$$

where $l$ is the optical path length, $\varepsilon_i^{\lambda}$ is the molar absorption coefficient and $c_i(t)$ is the concentration of the $i$th absorbing species out of $r$ species in the reaction mixture.

As the kinetic information is contained in the instantaneous function $f^{\lambda}(t)$, evaluation of the ultrafast kinetic data always includes a deconvolution, which provides the solution of the integral Eqs. (1) or (2) in the form of the (non-convolved) instantaneous $f^{\lambda}(t)$ function. This deconvolution is usually performed implicitly, by fitting the convolution of a suitable model function describing $f^{\lambda}(t)$ as a function of kinetic and photophysical parameters to measured experimental data (for example, see Keszei et al., 1995). Though this method gives probably the best deconvolved data set, as the functional form of the model constrains the deconvolution, it cannot be used if there is no reasonable kinetic model available. The aim of this paper is to describe some direct deconvolution methods based on inverse filtering via Fourier transforms of the measured $A^{\lambda}(\tau)$ and the effective pulse that can be used to obtain reasonable kinetic response functions from ultrafast kinetic experiments without any reference to a physical model. Fourier transform methods to treat ultrafast kinetic data are mentioned in earlier papers as well (for example, see McKinnon et al., 1977; O'Connor et al., 1979), but their use is also based on a supposed model function.

## 2. Numerical methods

Let us denote the effective pulse by $s(t)$, the instantaneous kinetic response by $f(t)$, and the resulting convolution—the measured absorbance as a function of the delay $\tau$ between the pump and the probe pulse—by $a(\tau)$. The relevant convolution equation can then be written as

$$a = s \otimes f. \tag{4}$$

Convolution does not have an inverse operation in the time domain. However, if we rewrite Eq. (4) by substituting the Fourier transforms of the functions defined as

$$F(\omega) = \frac{1}{\sqrt{2\pi}} \int_{-\infty}^{\infty} f(t) e^{-i\omega t} \, dt, \tag{5}$$

then we get a simple expression for the convolution in the frequency domain (as a function of the angular frequency $\omega$):

$$A = SF. \tag{6}$$

As convolution becomes simple multiplication in the frequency domain, its inverse can readily be written as

$$F = \frac{A}{S}. \tag{7}$$

In terms of digital signal processing, Eq. (6) can be considered as the digital filtering of $F$ by the filter $S$, which explains why Eq. (7) is called inverse filtering (for example, see Hamming, 1989).

A serious problem with the deconvolution using the inverse filtering method arises from the noise content of $A$ originating from the experimental error in the measured $a$ function. As both $s$ and $f$ are slowly varying functions, their Fourier transforms $A$ and $S$ contain large amplitudes at low frequencies, but very low amplitudes at high frequencies. Thus, the ratio $A/S$ becomes practically zero divided by zero (except for the noise), so division by zero largely enhances the noise content of $A$. In principle, inverse Fourier transformation of the deconvolved $F$ defined as

$$f(t) = \frac{1}{\sqrt{2\pi}} \int_{-\infty}^{\infty} F(\omega) e^{i\omega t} \, d\omega \tag{8}$$

should lead to the instantaneous kinetic function $f$, but in fact the noise enhancement results in an $\hat{f}$ function whose noise content is typically larger by several orders of magnitude than the signal amplitude itself. We can overcome this difficulty by a properly chosen additional filter that would remove the noise while keeping the information content concerning the instantaneous kinetic function $f$:

$$\hat{F} = K \frac{A}{S}. \tag{9}$$

Here, $K$ is the searched-for filter function, and $\hat{F}$ is the result of deconvolution, both in the frequency domain. However, due to the noise content of $A$, Eq. (9) does not provide a unique solution, so we should include some additional constraints to get an $\hat{F}$ function that leads to an acceptable $\hat{f}$ in the time domain.

In this paper, we show deconvolution results obtained with additional Wiener filtering or regularization. A Wiener filter is the one that minimizes the sum of squared differences between the original function $f$, and the inverse Fourier transform of $\hat{F}$, denoted by $\hat{f}$. As the original $f$ function is not known, approximations for the optimal Wiener filter are usually used. In the case of a white noise—where the noise amplitude is the same constant $N$ at each frequency—the Wiener filter can be approximated with the form (Gobbel and Fike, 1994)

$$W = \frac{|A|^2}{|A|^2 + |N|^2 / |S|^2}. \tag{10}$$

The relevant implementation of this filter to get the deconvolved $\hat{F}$ is

$$\hat{F} = \frac{|A|^2}{|A|^2 + |N|^2/|S|^2} A \frac{1}{S}. \tag{11}$$

This filter—called *modified adaptive Wiener filter*—has been successfully used to deconvolve radioactive indicator-dilution response curves by Gobbel and Fike (1994).

Regularization filters have been developed after Tikhonov and Arsenin (1977) proposed them to treat ill-posed problems—such as deconvolution of noisy data. We have implemented a two-parameter filter used by Dabóczi and Kollár (1996) of the form

$$R = \frac{|S|^2}{|S|^2 + \lambda + \gamma|L|^2}, \tag{12}$$

which gives the deconvolved $\hat{F}$ according to the formula

$$\hat{F} = \frac{AS^*}{|S|^2 + \lambda + \gamma|L|^2}. \tag{13}$$

Here,

$$|L(\omega)|^2 = 16\sin^4\left(\frac{\pi\omega}{\omega_s}\right) \tag{14}$$

is the square of the absolute value of the Fourier transform of the second-order backward differential operator, and $S^*$ means the complex conjugate of the frequency domain function $S$. Regularization has been applied to isothermal DSC data by Pananakis and Abel (1998) using the equivalent of Eq. (12) with $\gamma = 0$, i.e., using only a one-parameter regularization filter.

Both methods mentioned above contain optimization of parameters. In the Wiener filter, the noise power $|N|^2$, while in the regularization filter, the parameters $\lambda$ and $\gamma$ are to be optimised. There is an additional difficulty compared to applications of Fourier-transform-based methods reported in the literature, namely, the non-periodical nature of the data sets, as can be seen from Fig. 1. It makes the Fourier transforms have virtual high-frequency components, as the difference from zero at the end of the data sets means a discontinuity in a circular transformation, which generates frequency components characteristic of steplike functions. The actual discrete numeric transformation of the data sets was made either by fast Fourier transformation (FFT) using zero padding of the 136 data points up to 256, or using a direct Fourier transformation [DFT, performing the operations of Eq. (5)] of the 136 points only, without zero padding. This latter method gave very much spurious deconvolved result, unless we constructed strictly periodic functions by doubling the original data set and putting together the two "copies" in a suitable way (see Gans and Nahman, 1982).
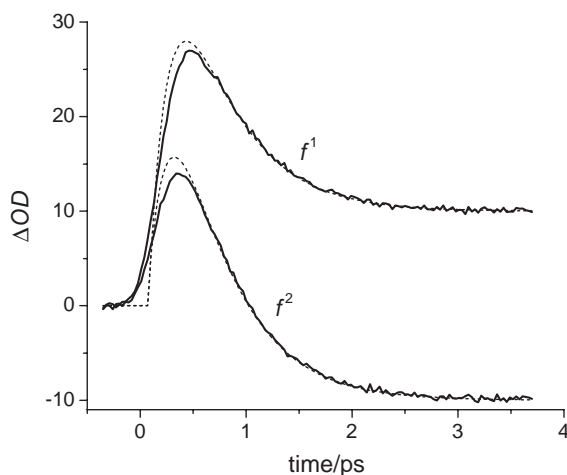


Fig. 1. Simulated ultrafast kinetic curves used to test deconvolution methods. Dashed curves show the noiseless instantaneous kinetic responses, and solid curves are convolved with a 255 fs FWHM Gaussian pulse with error added to mimic measured experimental curves.

To test the applicability of the methods for typical ultrafast laser data sets, we have performed the deconvolution of simulated kinetic curves. The two curves used were calculated from the solution of the differential equations of the simple consecutive reaction

$$A \xrightarrow{\tau_1} B \xrightarrow{\tau_2} C \tag{15}$$

with the initial conditions $[A] = 1 \, \text{mol dm}^{-3}$, $[B] = [C] = 0$ at $t = 0$. The resulting kinetic response functions can be written as

$$\begin{aligned}
f^\lambda(t) = {} & \varepsilon_A^\lambda e^{-t/\tau_1} + \varepsilon_B^\lambda \frac{\tau_2}{\tau_1 - \tau_2}(e^{-t/\tau_1} - e^{-t/\tau_2}) \\
& + \varepsilon_C^\lambda\left(1 + \frac{\tau_2 e^{-t/\tau_1} - \tau_1 e^{-t/\tau_2}}{\tau_1 - \tau_2}\right).
\end{aligned} \tag{16}$$

The time constants were set at $\tau_1 = 200 \, \text{fs}$ and $\tau_2 = 500$ fs. One of the curves has a partial recovery of the transient absorbance with the parameters $\varepsilon_A^1 = 5$, $\varepsilon_B^1 = 45$ and $\varepsilon_C^1 = 10$ (all the molar absorptivities $\varepsilon_i^\lambda$ are in $\text{dm}^3\,\text{mol}^{-1}\,\text{cm}^{-1}$ units). The other curve has a permanent bleaching after the completion of reaction (15), with the parameters $\varepsilon_A^2 = 5$, $\varepsilon_B^2 = 30$ and $\varepsilon_C^2 = -10$. To mimic experimental ultrafast kinetic data, we have convolved both $f^\lambda$ functions with a 255 fs FWHM Gaussian pulse, sampled it at 30 fs intervals, and added a normally distributed error with a variance of 2% of the maximum of each data set (see Fig. 1).

Optimizations were done using a grid search in one (Wiener filter and one-parameter regularization) and in two dimensions (two-parameter regularization), monitoring different parameters that could be used as

optimum criteria. One of the best criteria is always the root-mean-square (RMS) error of the deconvolved $\hat{f}$ with respect to the undistorted $f$ function (which is known in the case of simulated data) calculated as

$$RMS_{\text{diff}} = \sqrt{\frac{\sum\limits_{i=1}^{m}(f_i - \hat{f}_i)^2}{m-1}}, \tag{17}$$

where $m$ is the number of data. From the point of view of kinetic inference, a better indicator is the estimation of the kinetic and photophysical parameters $\tau_1$, $\tau_2$ and the $\varepsilon_i^\lambda$ values, compared to the (known) original parameters used to generate the simulated data sets. We have performed parameter estimations using a global non-linear fit of the model function (16) to the deconvolved data using the Marquardt algorithm (Marquardt, 1963; see also Keszei et al., 1995). Residual errors after the optimal fit also indicate the quality of deconvolution. Comparing estimated parameters to their original value indicates also systematic deviations from the true value. A systematic error in the parameters is also indicated by the Durbin–Watson D-statistics (Durbin and Watson, 1950, 1951; see also Turi et al., 1997).

If we evaluate real experimental data, we do not know the undistorted $f$ functions, nor the true values of the parameters. As the reason for using direct deconvolution is the lack of a reasonable kinetic model, we cannot use a model function to fit deconvolved data either. That is why we were looking for statistics to indicate optimum criteria using only the measured data set $a$ and the deconvolved $\hat{f}$ data set. An obvious statistics is the RMS error of the reconvolved $\hat{a} = \hat{f} \otimes s$ with respect to the measured $a$ data set, defined analogously to Eq. (17) [in the case of an ideal (exact) deconvolution, $\hat{a}$ should be identical to the (noisy) experimental $a$ data set]. As a fundamental problem in deconvolution is the amplified noise, a noise indicator would be a good candidate as well to control the optimization parameters. An ingenious indicator has been proposed by Gobbel and Fike (1994), named oscillation index, which measures the additional noise superposed on an ideally smooth unimodal curve:

$$OSC = \frac{\sum\limits_{i=1}^{m}\left|\hat{f}_i - \hat{f}_{i-1}\right| - 2\hat{f}_{\text{max}} - \hat{f}_1 - f_m}{m(\hat{f}_{\text{max}} - \hat{f}_{\text{min}})}, \tag{18}$$

where $\hat{f}_1$ is the minimum of the data set before $\hat{f}_{\text{max}}$, the maximum, and $\hat{f}_m$ is the minimum after $\hat{f}_{\text{max}}$. Intuitively, we would prefer a deconvolved data set with a noise content—i.e., with an OSC—not greater than that of the measured $a$ data set.
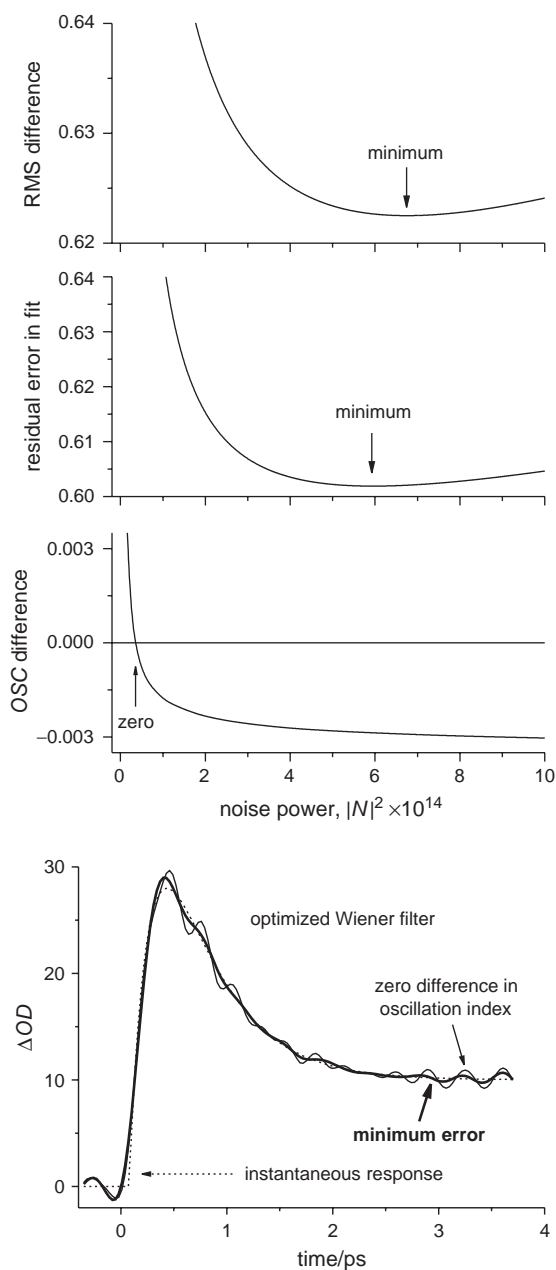


Fig. 2. Top: optimum criteria as a function of the noise parameter $|N|^2$ of the Wiener filter. Bottom: deconvolved $\hat{f}^1$ data set obtained at the minimum RMS error with respect to the instantaneous function (thick solid line), and at zero difference of the oscillation index with respect to the "measured" data (thin solid line). For comparison, the noiseless instantaneous response function (dashed line) is also shown.

## 3. Results and discussion

We have performed a grid search on a suitably fine grid while optimizing filter parameters during the

deconvolution of the data sets described in the previous section. Fig. 1 shows the simulated data sets, compared to the respective (noiseless) instantaneous response functions.

In case of the Wiener filter, there is one parameter to optimize, so the change of the optimum criteria can easily be shown in a one-dimensional plot as a function of the noise power $|N|^2$. As we can see from Fig. 2, there is a minimum of the RMS error of the deconvolved data set with respect to the (noise free) instantaneous data, and another minimum of the residual errors in a least-squares fit of the (known) model function to the deconvolved data set. The two minima are found to be quite close to each other ( $|N|_{\text{diff}}^2 = 6.74 \times 10^{-14}$ and $|N|_{\text{res}}^2 = 5.95 \times 10^{-14}$ for $\hat{f}^1$; $|N|_{\text{diff}}^2 = 3.24 \times 10^{-14}$ and $|N|_{\text{res}}^2 = 2.83 \times 10^{-14}$ for $\hat{f}^2$), and there is no visible difference between the graphs of the deconvolved data according to the two different minima (accordingly, the respective RMS errors are also very close to each other).

The plot of the RMS error of the reconvolved data set with respect to the "measured" data does not show a minimum within the studied range of $|N|^2$. It increases monotonically with increasing $|N|^2$, indicating the ill-posed nature of deconvolution. This means that the large high-frequency noise generated by simple inverse filtering completely disappears when we reconvolve the noisy $\hat{f}$ data set, and the increase in error follows the distortion of $\hat{f}$ caused by the suppression of higher frequencies. The above results were obtained with the DFT method using doubling of the data set to make it periodic. When using simple FFT !with zero padding, we have got similar deconvolution results but somewhat more spurious curves. Accordingly, the optimal $|N|^2$ parameter to control noise is larger by several orders of magnitude; close to $10^{-4}$. However, apart from a more spurious behaviour, the deconvolved curve is quite close to that obtained with DFT.

The oscillation index OSC also changes monotonically with $|N|^2$, in accordance with the above statements. However, in this case we have a critical noise indicator, the oscillation index of the "measured" data, which poses; a natural limit to the monotonous decrease of the noise with increasing $|N|^2$. Obviously, there is no reason to decrease the noise much further once we have attained the same noise level in the deconvolved $\hat{f}$ function as that of the original data to deconvolve. As can be seen in Fig. 2, this particular value of the oscillation index is attained for fairly lower $|N|^2$, i.e., for lower noise suppression than the optimal $|N|_{\text{diff}}^2$ and $|N|_{\text{res}}^2$ values. Thus, the difference of the oscillation index of the deconvolved and the measured data sets is a useful *lower threshold indicator* for the optimal $|N|^2$ parameter of the Wiener filter in these data sets.
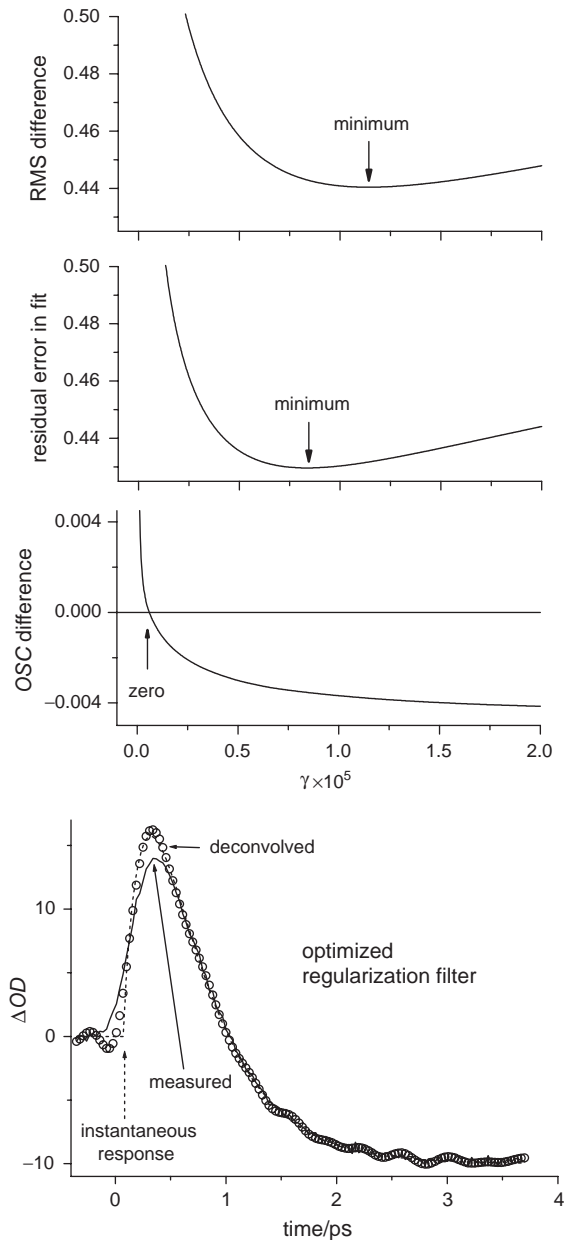


Fig. 3. Top: optimum criteria as a function of the regularization parameter $\gamma$. Note that the two-parameter optimum was obtained with $\lambda = 0$, so only the variation of the criteria as a function of $\gamma$ is shown. Bottom: deconvolved $\hat{f}^2$ data set (circles) obtained with optimized $\gamma$ [same as with two-parameter regularization using Eq. (13)]. For comparison, the instantaneous response function (dashed line) and the simulated "measured" curve (solid line) are also shown.

In the case of regularization, we can have a choice between one-parameter optimizations of either $\lambda$ and $\gamma$, or a two-parameter optimization of both parameters. If we extend our two-dimensional grid search down to

$\lambda = 0$ and $\gamma = 0$, as well as up to high enough values to attain the optimum of one parameter if the other one is zero, we can have optimal values for all the three cases. The results of grid search are similar, as described with the Wiener filter. The RMS difference of the instantaneous and the deconvolved data, along with the residual error when fitting the model function show minima over the variables $\lambda$ and $\gamma$, while the difference of the oscillation indices of the deconvolved and the "measured" data sets varies monotonically, but attains zero not far from the above-mentioned two optima. Here, there is a greater difference using FFT and DFT. When using FFT with zero padding, the optimum is found at nonzero $\lambda$, with a $\gamma/\lambda$ ratio close to 25. However, with the doubled periodic data set and DFT, the optimum is found at $\lambda = 0$, and with $\gamma$ values close to $1 \times 10^{-5}$ (while the optimal $\gamma$ with FFT and zero padding was a few times $10^{-2}$). This means that the contribution of the $\lambda$ parameter (i.e., smoothing the data set) is negligible in optimal noise reduction compared to the contribution of the $\gamma$ parameter (i.e., smoothing the derivative of the data set) if we avoid excessive spurious features. Fig. 3 summarizes the results obtained with the doubled periodic data set and DFT showing zero oscillation index difference, and the optimal values obtained for the two error criteria. Again, a zero oscillation index is a lower threshold value of the parameters for optimal smoothness of the deconvolved data set.

To compare the efficiency of inverse filtering deconvolution with the two different additional noise filters, parameter estimation results shown in Table 1 can also be considered. These results along with the visual inspection of the deconvolved curves support the fact that inverse filtering is a promising alternative to the model-based reconvolution to obtain undistorted instantaneous kinetic data if there is no reasonable kinetic and/or photophysical model available. The distortion of a Wiener filter is found to be somewhat more important

than that of regularization, which gives excellent parameters for the characteristic times, very good ones for the molar absorptivities of the species B and C. This method only fails at the absorptivities of the very shortly living transient A, whose absorptivities are also quite low compared to that of the longer living species.

The only optimum criterion that can be used in case of experimental data—where neither the underlying instantaneous data set $f$ nor its model function are known—is the difference between the oscillation index OSC of the measured and the deconvolved data sets. However, its optimal value seems to be not at zero difference for the present data sets, but at somewhat lower oscillation index of the deconvolved data, i.e., at a greater reduction of the noise by additional filtering. The level of optimal (negative) value of this difference can be decided by visual inspection of the deconvolved curves.

We have also checked the two methods by performing a deconvolution of experimental data measured by Barthel et al. (2003). Measured data shown in Fig. 4 were obtained for the electron detachment reaction of the CTTS state of sodide ($Na^-$) ions in THF solution, using the same Gaussian pulse shape with an experimentally determined pulse width as in the analysis of the data reported in the original paper. The quality of the deconvolved data set also supports the applicability of inverse filtering in the direct deconvolution of real experimental ultrafast kinetic data prior to kinetic and photophysical inference. Wiener filtering using the zero OSC difference criterion gives a fairly good deconvolved data set with the filter parameter $|N|^2 = 1 \times 10^{-10}$. However, as mentioned before, this is a lower threshold only for optimal filtering. If we perform further optimization by visual inspection, it is enough to increase this parameter to $|N|^2 = 1 \times 10^{-9}$ to get the "optimal" deconvolved data set shown in the top diagram of Fig. 4. Similarly, a 15-fold increase of the $\gamma = 8.2 \times 10^{-6}$ obtained for zero OSC difference gave the

Table 1

Estimated parameters obtained when fitting model function (16) to both deconvolved simulated data sets simultaneously

| Parameter | True value | Wiener filter | Regularization, optimized $\lambda$ | Regularization, optimized $\gamma$ |
|---|---|---|---|---|
| $\tau_1$ | 0.20 | 0.19 (0.02) | 0.20 (0.03) | **0.19 (0.02)** |
| $\tau_1$ | 0.50 | 0.49 (0.04) | 0.49 (0.04) | **0.50 (0.04)** |
| $\varepsilon_A^1$ | 5 | *8.6 (1.1)* | 8.8 (1.1) | ***8.7 (1.0)*** |
| $\varepsilon_B^1$ | 45 | 43.6 (2.2) | 43.3 (2.4) | **43.5 (2.1)** |
| $\varepsilon_C^1$ | 10 | 10.1 (0.2) | 9.9 (0.2) | **10.0 (0.2)** |
| $\varepsilon_A^2$ | 5 | ***7.3 (1.0)*** | *7.37 (1.0)* | *7.4 (1.0)* |
| $\varepsilon_B^2$ | 30 | *28.3 (1.7)* | 28.0 (1.8) | ***28.2 (1.6)*** |
| $\varepsilon_C^2$ | −10 | −9.9 (0.2) | −9.8 (0.2) | **−9.9 (0.2)** |

Characteristic times $\tau_1$ and $\tau_2$ are given in ps units, while molar absorptivities $\varepsilon_i^\lambda$ in $dm^3\,mol^{-1}\,cm^{-1}$. Numbers in italics indicate a systematic error in estimation. Bold numbers are the best estimates. Bold italics are the best estimates but with a systematic error. Headings indicate the additional noise filtering involved in deconvolution. Numbers in parentheses show the half widths of 95% confidence intervals.
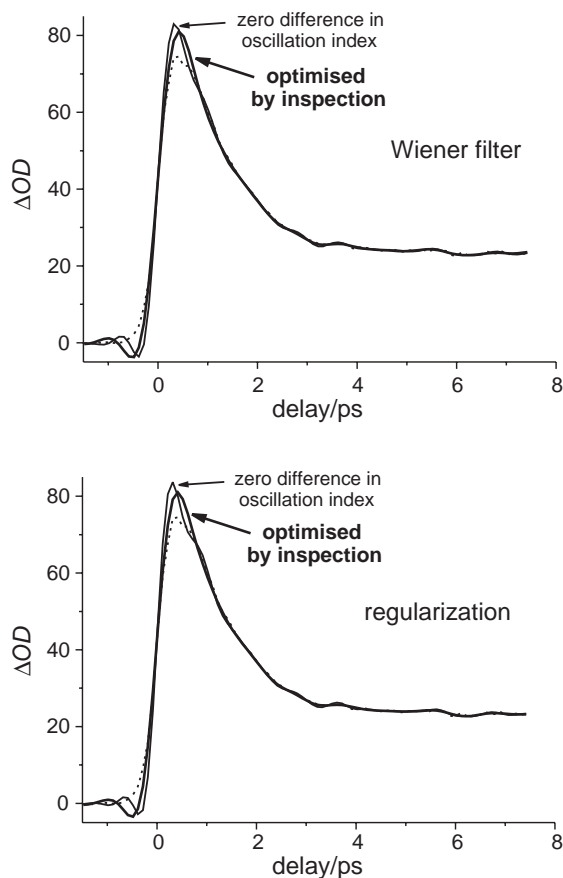
Fig. 4. Deconvolution results of experimental data sets measured for the electron detachment reaction of the CTTS state of sodide ($Na^-$) ions in THF solution at 490 nm. Top: slightly spurious Wiener-filtered deconvolution result obtained at zero difference of the oscillation index with respect to the measured data (thin solid line), and an ''optimally'' smoothed result found by visual inspection (thick solid line, less spurious). Bottom: deconvolution result obtained with optimized $\gamma$-parameter regularization at zero difference of the oscillation index with respect to the measured data (thin solid line), and an ''optimally'' smoothed result found by visual inspection (thick solid line). For comparison, the measured data set (thin dashed line) is also shown in both diagrams.

visual optimum with the regularization filter, shown in the bottom diagram.

As a result of this study, we can conclude that the direct deconvolution of ultrafast kinetic data can be performed using inverse filtering, via the Fourier transforms of the measured kinetic curve and the effective pulse. (The use is not restricted to ultrafast kinetics; it can be applied to any other experimental results where convolutive distortion cannot be avoided.) The non-periodic nature of the data sets to deconvolve seems not to pose problems, especially if we avoid zero padding using DFT and doubling of the data set, arranged in a

way to get a periodic function (see Gans and Nahman, 1982). The experimental noise content can be handled using additional filtering. If the noise can be considered as a white noise, adaptive Wiener filtering is a good candidate, but regularization filtering is less sensitive to noise distribution and gives somewhat more reliable results when estimating kinetic and photophysical parameters of the studied system. The second derivative-based regularization (parameter $\gamma$) gives a better result than a constant term (parameter $\lambda$). A further study of direct deconvolution of ultrafast kinetic experimental data is carried out in our laboratory.

**Acknowledgements**

**References**

Barthel, E.R., Martini, I.B., Keszei, E., Schwartz, B.J., 2003. Solvent effects on the ultrafast dynamics and spectroscopy of the charge-transfer-to-solvent reaction of sodide. J. Chem. Phys. 118, 5916–5931.

Chase, W.J., Hunt, J.W., 1975. Solvation time of the electron in polar liquids. Water and alcohols. J. Phys. Chem. 79, 2835–2845.

Dabóczi, T., Kollár, I., 1996. Multiparameter optimization of inverse filtering algorithms. IEEE Trans. Instrum. Meas. 45, 417–421.

Donoho, D.L., Stark, P.B., 1989. Uncertainty principles and signal recovery. SIAM J. Appl. Math. 49, 906–931.

Durbin, J., Watson, G.S., 1950. Testing for serial correlation in least squares regression. I. Biometrika 37, 409–428.

Durbin, J., Watson, G.S., 1951. Testing for serial correlation in least squares regression. II. Biometrika 38, 159–178.

Gobbel, G.T., Fike, J.R., 1994. A deconvolution method for evaluating indicator-dilution curves. Phys. Med. Biol. 39, 1833–1854.

Gans, W.L., Nahman, N.S., 1982. Continuous and discrete Fourier transforms of steplike waveforms. IEEE Trans. Instrum. Meas. IM-31, 97–101.

Hamming, R.W., 1989. Digital Filters, third ed. Prentice Hall, Englewood Cliffs, NJ.

Keszei, E., Murphrey, T.H., Rossky, P.J., 1995. Electron hydration dynamics: simulation results compared to pump and probe experiments. J. Phys. Chem. 99, 22–28.

Marquardt, D.W., 1963. An algorithm for least-squares estimation of nonlinear parameters. J. Soc. Indus. Appl. Math. 11, 431–441.

McKinnon, A.E., Szabo, A.G., Miller, D.R., 1977. The deconvolution of photoluminescence data. J. Phys. Chem. 81, 1564–1570.

O'Connor, D.V., Ware, W.R., André, J.C., 1979. Deconvolution of fluorescence decay curves. A critical comparison of techniques. J. Phys. Chem. 83, 1333–1343.

Pananakis, D., Abel, E.W., 1998. A comparison of methods for the deconvolution of isothermal DSC data. Thermochim. Acta 315, 107–119.

Tikhonov, A.N., Arsenin, V.Y., 1977. Solutions of Ill-Posed Problems. V.H. Winston, Washington, DC.

Turi, L., Holpár, P., Keszei, E., 1997. Alternative mechanisms for solvation dynamics of laser-induced electrons in methanol. J. Phys. Chem. A 101, 5469–5476.